R. Venkatesh
K. Jayakumar ✉

https://doi.org/10.21278/TOF.502080825
ISSN 1333-1124
eISSN 1849-1391

INVESTIGATION OF MICROSTRUCTURE AND MECHANICAL PROPERTIES OF COLD METAL TRANSFERWELDED AA7075 JOINTS

Summary

This study investigates the mechanical performance and microstructural evolution of AA7075 aluminium alloy joints produced using the cold metal transfer process. Owing to its low heat input, cold metal transfer is well suited for welding heat-sensitive precipitation-hardened alloys prone to porosity, hot cracking, and strength loss. Response surface methodology with a central composite design was applied to quantify the effects of welding current (160 to 200 A), welding speed (100 to 140 mm/min), and wire feed speed (1000 to 2000 mm/min) on ultimate tensile strength. The resulting empirical model showed strong statistical significance and close agreement between predicted and experimental values. Microstructural analysis revealed the dissolution of dizinc magnesium precipitate, dendritic solidification, and inter-dendritic segregation in the fusion zone; partial over-ageing in the heat-affected zone; and the retention of the T6 structure in the base metal. Hardness decreased from 164–171 HV0.5 (the base metal) to 147–155 HV0.5 (the heat-affected zone) and 140–145 HV0.5 (the fusion zone). Validation using optimised parameters achieved an ultimate tensile strength of 366 MPa, matching the model prediction. Overall, the study confirms cold metal transfer as an effective technique for producing high-strength AA7075 welds with minimal thermal damage.

Key words: *AA7075; Cold metal transfer; Welding parameters; Response surface methodology; Microstructure; Hardness; Tensile strength*

1. Introduction

Aluminium alloys, especially of the 7xxx series, are extremely important in industries that require a high strength-to-weight ratio, e.g., the aerospace, motor and defence industries [1]. The AA7075 alloy has outstanding mechanical characteristics and corrosion resistance, which makes it a suitable material for such applications. However, the welding of AA7075 is very challenging due to its high propensity to hot cracking, porosity as well as significant loss of mechanical properties in the heat-affected zone [2]. These difficulties have led to the development and improvement of superior welding methods, which have the capacity to reduce instances of defects while maintaining the inherent properties of the alloy. Another promising process for joining AA7075 is cold metal transfer (CMT) welding, which is an improved version of gas metal arc welding (GMAW). The CMT process is characterised by high thermal control, which is achieved by a controlled system of wire feed and by a special method of

current modulation [3]. CMT also minimises the amount of thermal energy in the weld compared to traditional MIG welding, thereby minimising the distortion and increasing the quality of the weld [4]. The reduced amount of heat reduces thermal distortion and spatter; this makes CMT suitable for materials such as AA7075, which can be affected by extreme temperatures in such a way that they destroy the quality of the weld [5]. The effective use of CMT in the welding of AA7075 results in reduced distortion and a higher quality of the weld, but again, welding parameters have to be optimised carefully to attain the required mechanical performance and microstructure integrity [6].

The welding parameters, such as the welding speed, welding current, and wire feed rate, are of major importance for the success of the CMT welding of AA7075 alloys. These parameters have a significant effect on the amount of heat input, depth of penetration, and flow of the material during the welding; the latter is also considered a key factor in determining the quality of the weld. In this paper, the central composite design (CCD) of response surface methodology (RSM) will be used to monitor the impact of these parameters in a systematic way to determine the best conditions under which CMT welding is performed [7]. The RSM provides a sound statistical framework for modelling the interactions between the welding parameters, thus allowing for the prediction and optimisation of the results of welding in a range of settings [8]. The microstructure and mechanical characteristics of the CMT-welded AA7075 joints are thoroughly analysed after the optimisation process. In the microstructural analysis, the structure of the grain, the distribution of the phases, and possible defects (porosity or cracking) are determined [9]. At the same time, mechanical characteristics, such as tensile strength, hardness, and elongation, are measured to investigate how the optimised welding parameters affect the joint. Together with the optimised parameters, such assessments would play a crucial role in explaining the overall quality and longevity of the CMT-welded [10].

Wang Kekuan et al. [11] conducted a study on the CMT welding of AA7075 with the ER7075 wire and investigated the influence of electrode polarity and current waveforms on the molten metal transfer, appearance of the weld, and penetration. In more recent times, Babatunde Olamide Omiyale et al. [12] reported the great effect of using the best process parameters in the CMT-based wire arc additive manufacturing (WAAM) process on the mechanical and microstructural characteristics of different aluminium alloys. They showed that CMT has low heat production, which results in cleaner surfaces and lower spatter than GMAW.

The literature review indicates that there is a dearth in the research literature devoted to the CMT welding of the AA7075 alloy and that the current studies involve the overall effect of the three chosen welding parameters on the weld strength expressed through the RSM-CCD optimal method in terms of hardness and ultimate tensile strength (UTS). The results of this study are expected to extend the knowledge on how to achieve the optimal CMT welding process for AA7075. This study aims to contribute to the development of more effective and reliable welding methods for high-strength aluminium alloys by clarifying the relationships between welding parameters, microstructure, and mechanical properties. The results have the potential of being applied in industry to enable the production of high-quality welded joints, which will improve the performance and durability of AA7075 parts in a demanding environment.

2. Experimental Procedure

The experiment was done on AA7075 alloy plates to investigate the influence of cold metal transfer (CMT) welding parameters on the microstructure and the mechanical properties of welded joints. The methodology included the material characterisation, welding parameter selection, weld fabrication using an RSM-based design matrix, mechanical testing, and microstructural analysis.

2.1 Base material characterisation

The base material used in this study was the AA7075-T6 aluminium alloy with a plate thickness of 5 mm. The plates were machined to dimensions of 100 mm × 60 mm. The chemical composition of the alloy was determined using an optical emission spectrometer (OES), produced by Foundry-Master Pro, Oxford Instruments, and calibrated using certified reference standards. The measured elemental composition is given in Table 1.

Table 1 Elemental composition of base material (wt.%)

Parent metal	Zn	Mg	Mn	Cu	Cr	Fe	Si	Ti	Al
AA7075	5.6	2.4	0.2	1.2	0.2	0.3	0.2	0.1	89.8

Mechanical properties of the base material were evaluated through tensile testing according to ASTM E8/E8M. Flat dog-bone specimens were extracted along the rolling direction at room temperature (≈25 °C). The resulting values of ultimate tensile strength (σ_UTS), yield strength (σ_YS), Vickers hardness (HV), and percent elongation (% El) are shown in Table 2.

Table 2 Base material mechanical properties

Parent metal	Vickers hardness	UTS (MPa)	YS (MPa)	% El
AA7075	171	568	493	9

2.2 Selection of welding parameters

Three primary CMT welding parameters were selected: welding current (I, A), welding speed (V, mm/min), and wire feed speed (V_f, mm/min). A preliminary set of trial welds was produced to identify workable parameter boundaries by examining weld penetration, bead appearance, and macrostructural integrity. Based on the literature data [13] and the findings of trial welds, appropriate limits for each parameter were established, and coded levels (−1.682 to +1.682) were assigned in accordance with the CCD of the RSM.

2.3 Welding setup

Welding was performed using a Fronius TransPuls Synergic 3200 CMT system equipped with a robotic arm to ensure consistent weld bead placement; the system is shown in Figure 1. The plates were cleaned with acetone to remove contaminants and securely clamped in a butt-joint configuration as shown in Fig. 2(a). Welding was carried out using pure argon shielding gas at a flow rate of 15 L/min. A single-pass weld was deposited for each parameter combination defined by the RSM matrix. Cross-sectional macrographs were obtained for each weld bead after standard metallographic preparation to verify fusion, bead shape, and the presence of defects.

2.4 Tensile testing

Transverse tensile specimens were taken across the weld according to ASTM E8/E8M using wire electrical discharge machining (WEDM). Three specimens were prepared for each weld (n=3) to ensure repeatability. The specimen geometry is shown in Fig. 2(b). Testing was performed using a Bluestar LDW-50 universal testing machine at a crosshead speed of 0.5 mm/min.

Fig. 1 CMT welding setup with a robotic arm

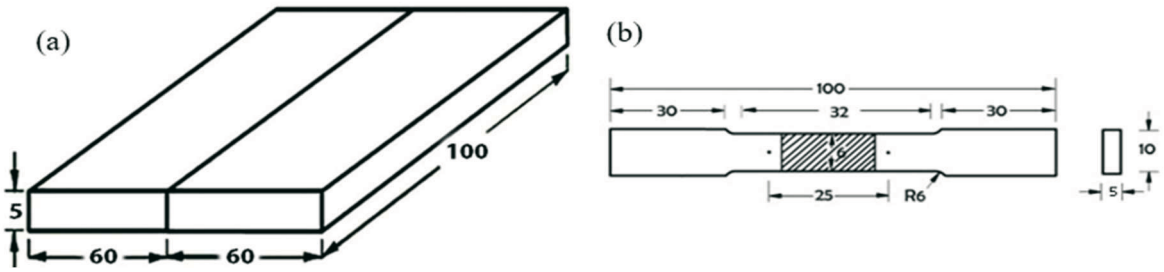

Fig. 2 a) Schematic of the single butt configuration b) Configuration of a tensile specimen

2.5 Microstructural analysis

For microstructural examinations, specimens were taken perpendicular to the weld. The specimens were mounted using phenolic powder, followed by sequential grinding (80–2500 grit) and polishing with 1 μm diamond suspension. Barker's reagent was used for etching. Scanning electron microscopy (SEM) was conducted using a ZEISS EVO 18 system. Grain size in the base metal, fusion zone, and heat-affected zone was quantified using the line-intercept method in accordance with ASTM E112. Precipitate size and volume fraction were estimated using the ImageJ software with calibrated thresholding techniques.

2.6 Hardness measurement

Vickers microhardness measurements were carried out across the weld cross-section using an ESEWAY EW-423 DAP microhardness tester. A test load of 500 gf (HV0.5) was applied with a dwell time of 20 s. Although ASTM E384 recommends 10–15 s dwell time, a longer duration was adopted to ensure stable indenter penetration in the soft aluminium fusion zone; similar dwell extensions have been reported in aluminium welding literature [14-16]. Indentations were placed at 1 mm intervals across the BM–HAZ–FZ regions, and the resulting hardness profile was plotted.

2.7 RSM design and experimental matrix

The CCD model included 20 experimental runs, comprising eight factorial runs, six axial runs, and six centre-point repeats, to assess curvature and pure error. Empirical model development and ANOVA validation are presented in Section 3.

3. Results and Discussion

The results and discussion section provides a comprehensive evaluation of the weld quality, statistical modelling, mechanical behaviour, and microstructural behaviour of AA7075 joints made using cold metal transfer (CMT), focusing on the variations in welding parameters.

3.1 Fixing the limits for welding parameters

Determining the practical and physically significant parameter limits for welding current (I), welding speed (V), and wire feed speed (V_f) is essential for ensuring that welds remain defect-free and representative of good industrial practice. A series of preliminary weld trials was performed to map the operating window of the CMT process for AA7075, focusing on bead morphology, penetration, arc stability, and macrostructural integrity. At lower heat-input conditions (low I or high V), common issues included incomplete fusion, insufficient penetration, and underfilled joints, consistent with observations from aluminium CMT welding in prior studies [3,4]. Conversely, excessive heat input (high I or low V) generated localised melt instability, wider softening zones, increased porosity, and evidence of filler burn-off. These types of behaviour align with thermal gradients and solute evaporation effects reported for Zn–Mg–Cu alloys in [17,18]. Representative macrographs used during limit establishment are shown in Figure 3. Based on trial observations and related literature, the selected limits (−1.682 to +1.682 coded levels) provided a robust envelope for RSM. The actual values associated with these levels are given in Table 3.

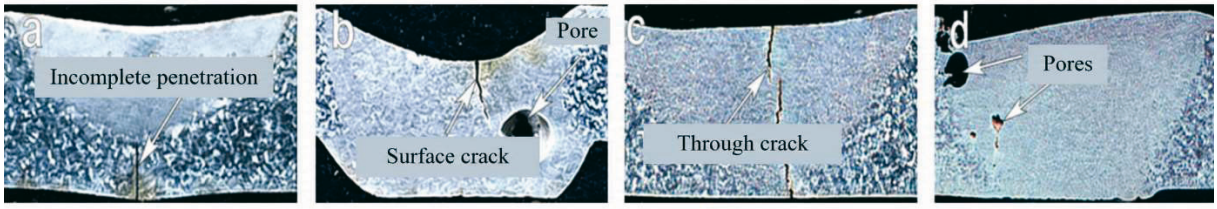

Fig. 3 Macrostructure of welding trials conducted to establish the welding limit

Table 3 Limits of welding process parameters

WPP	Short name	Levels				
		-1.682	-1	0	1	1.682
Welding current (A)	I	160	168	180	192	200
Welding speed (mm/min)	V	100	108	120	132	140
Wire feed rate (mm/min)	V_f	1000	1203	1500	1797	2000

3.2 Development of empirical relationship using the response surface method

The RSM is the unification of statistical and mathematical approaches suited for simulating and evaluating situations. From the experimental results, the following prediction equations were obtained (equation 1 with coded and equation 2 with actual factors). The equation in terms of actual factors can be used to anticipate the reaction at various degrees of each factor. The levels should be provided in original units of each factor [19]. The experimental design matrix and corresponding ultimate tensile strength values (σ_UTS) are shown in Table 4.

$$\text{Tensile strength (MPa)} = C_0 + C_1(I) + C_2(V) + C_3(V_f) + C_4(I*V) + C_5(I*V_f) + C_6(V*V_f) + C_7(I^2) + C_8(V^2) + C_9(V_f^2) \quad (1)$$

$$\text{Tensile strength (MPa)} = +363.32 - 10.1(I) + 8.45(V) - 5.196(V_f) + 1.875\ (I \times V) + 0.875\ (I \times V_f) - 2.125\ (V \times V_f) - 8(I^2) - 7.82(V^2) - 9.77\ (V_f^2) \quad (2)$$

Table 4 Design matrix with tensile strength and fusion zone area values

Std. order	Run order	Coded values			Real values			UTS-σ (MPa)
		I	V	V_f	Welding current (I) (A)	Welding speed (V) (mm/min)	Wire feed rate (V_f) (mm/min)	
1	20	-1	-1	-1	168	108	1203	345
2	11	1	-1	-1	192	108	1203	320
3	8	-1	1	-1	168	132	1203	362
4	12	1	1	-1	192	132	1203	344
5	16	-1	-1	1	168	108	1797	338
6	18	1	-1	1	192	108	1797	316
7	9	-1	1	1	168	132	1797	346
8	1	1	1	1	192	132	1797	332
9	15	-1.682	0	0	160	120	1500	358
10	13	1.682	0	0	200	120	1500	323
11	14	0	-1.682	0	180	100	1500	326
12	7	0	1.682	0	180	140	1500	356
13	10	0	0	-1.682	180	120	1000	345
14	5	0	0	1.682	180	120	2000	326
15	19	0	0	0	180	120	1500	363
16	3	0	0	0	180	120	1500	366
17	4	0	0	0	180	120	1500	362
18	6	0	0	0	180	120	1500	364
19	2	0	0	0	180	120	1500	363
20	17	0	0	0	180	120	1500	363

The presence of significant quadratic terms reflects curvature in the design space, indicating that peak performance lies at intermediate, not extreme, parameter values. This agrees with the prior RSM-based aluminium welding models [7, 20]. After welding, the macrostructure of all 20 welded specimens was analysed to understand the weld quality and zones; the macrostructures are shown in Figure 4.

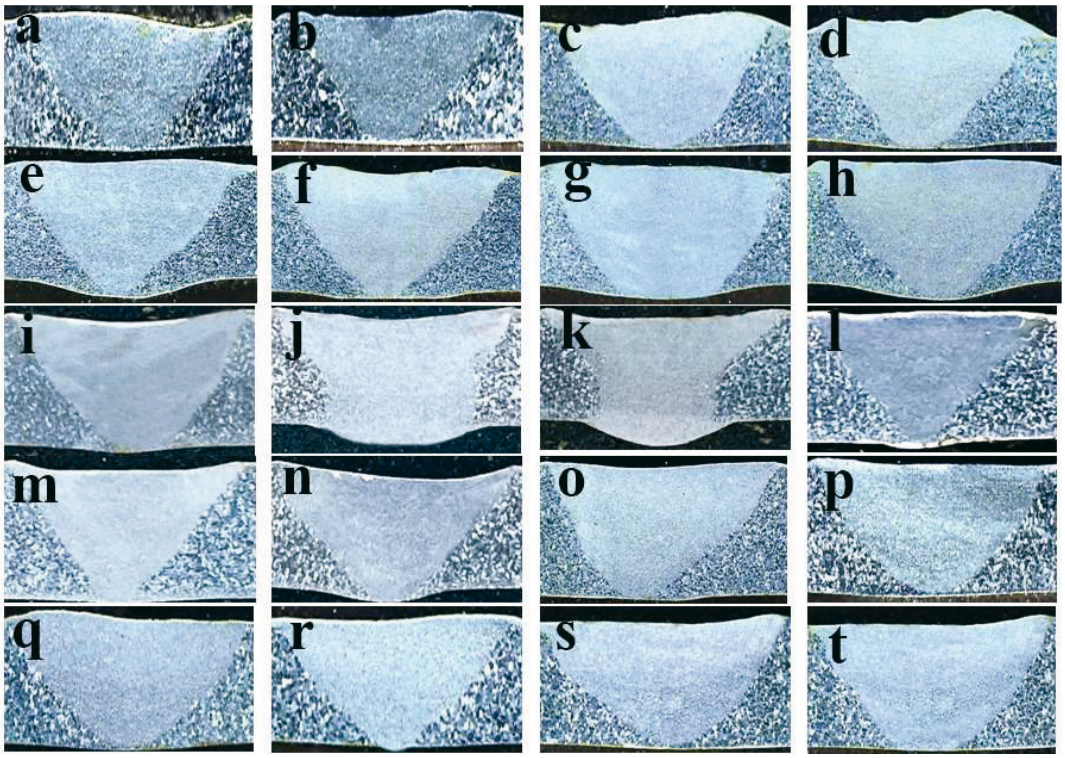

Fig. 4 Macrostructure of the welded specimens

3.3 Validation of the formed empirical relation

ANOVA results (Table 5) confirm that the developed model is statistically robust. The high Model F-value (>550) and the low p-value (<0.0001) signify that the regression is highly significant. All primary factors (I, V, V_f), two-factor interactions, and quadratic terms were statistically significant. The physical significance of the parameter sensitivity is as follows. Welding current (I) showed the strongest influence due to its direct role in heat input, droplet detachment dynamics, and arc force. In the prior CMT studies, the welding current (I) was identified as the dominant factor in the thermal and mechanical behaviour of aluminium welds [21, 22]. Welding speed (V) ranked second in influence. Since the heat input is inversely proportional to ($Q \propto VI/v$), lower speeds result in excessive heat accumulation, a wider HAZ, and grain coarsening. Wire feed speed (V_f) was the least influential because, although it affects deposition rate and arc length corrections, it has minimal direct impact on thermal gradients. The strong agreement between the predicted R^2 (0.9609) and adjusted R^2 (0.9662) validates the predictive capability of the model, further supported by almost no lack of fit value.

Table 5 Results obtained from ANOVA

Source	Sum of squares	df	Mean square	F-value	p-value	
Model	5467.69	9	607.52	559.52	< 0.0001	significant
A-I	1391.69	1	1391.69	1281.73	< 0.0001	
B-V	976.04	1	976.04	898.92	< 0.0001	
C-V_f	368.64	1	368.64	339.51	< 0.0001	
AB	28.13	1	28.13	25.90	0.0005	
AC	6.13	1	6.13	5.64	0.0389	
BC	36.13	1	36.13	33.27	0.0002	
A^2	922.03	1	922.03	849.18	< 0.0001	
B^2	881.72	1	881.72	812.06	< 0.0001	
C^2	1374.61	1	1374.61	1266.00	< 0.0001	

3.4 Trend analysis of ultimate tensile strength (UTS) concerning the welding current (I), welding speed (V), and wire feed speed (V_f)

The effects of varying values of the input parameters on ultimate tensile strength (UTS) are well depicted in the perturbation plot (Fig. 5(a)); the values of one parameter are varied while the values of the other two parameters are held constant at their centric values. This form of representation shows the parameter-dependent contributions of each parameter to the mechanical properties of the weld and enables a better insight into the individual effects of parameters. Plot 5a shows the effect of the change in I from 160 to 200 A by keeping the other two parameters, i.e., V and V_f, at the centric points. At the I of 160 A, the UTS is low at around 357 MPa, but when the value of I increases to about 174 A, the UTS increases to around 366 MPa. Further increase in the value of I softens the fusion zone through grain coarsening, precipitate dissolution, and evaporation of Mg–Zn strengthening elements; this is consistent with the earlier findings for 7xxx Al alloys [23, 1]. When there is an excessive heat input, some phenomena, such as dissolution of precipitates and increase in grain size, occur, resulting in reduced UTS. A similar phenomenon occurs in the case of the V-plot, with the only difference being that the heat input is inversely proportional to V. In the case of wire feed rate, if it is low, the filler will not be sufficient to fill the gaps; this fact results in voids inside the weldment, so an optimal V_f is required for a strong joint.

The arc length correction also plays a major role in the strength of the CMT weldment. Welding current in the CMT process is relatively less strong than in conventional MIG/MAG processes [21]. As the current directly affects the arc force and thermal input, its effect on the

arc length is significant. At stronger welding currents, increased arc energy will lead to excessive arc elongation unless corrected. The CMT system compensates for that by reducing the wire feed speed or increasing the retraction speed to ensure the arc length stability [22]. At less strong welding currents, the arc is narrowed, and the system compensates for that by feeding the wire faster or reducing the retraction [23].

The welding speed (V) exhibited an inverse but symmetric effect: high welding speed reduced the heat input and caused poor fusion, while extremely low welding speed delivered excessive heat, enlarging the HAZ and reducing strength. Increased welding speed results in the arc being quickly moved away from the weld pool, thus decreasing the heat input per unit length and reducing the possibility of arc instability or insufficient fusion. Arc length correction has to be done quickly to ensure a constant distance and prevent arc extinction. At lower welding speeds, the arc over the weld pool is longer with the possibility of creating even a longer arc and greater heat input. The CMT system avoids the occurrence of this phenomenon by actively managing the wire retraction to enable a shorter and controlled arc length. The wire feed speed (V_f) controlled the filler deposition and arc stability. Lower V_f caused incomplete filling and microporosity; excessive V_f produced arc length instability and inconsistent droplet transfer. In CMT, this control has a direct correlation with the mechanical retraction system. Increasing wire feed rates causes the filler wire to approach the molten pool at a faster rate, causing the arc to be made shorter unless actively counteracted by retraction. The arc length correction system increases the retraction speed to ensure arc stability. Decreasing wire feed rates slows the filler wire approach rate, causing the arc to be made longer. The system compensates for that by slowing retraction or increasing forward wire feed to restore the target arc length.

Equally, the contour plots (Fig. 5(b-d)) show the interactive impacts of two input parameters on UTS when the third parameter remains at its centric position [24]. These images are essential in the determination of the synergetic links reserved to parameters and overall effect on the quality of the weld [25]. The welding current and the welding speed have a significant impact on heat input, which is an important factor in determining the tear weld characteristics. The relationship between heat input and current in welding is linear, i.e., the stronger the current is, the larger is the heat input, and therefore, there is a possibility of expansion of heat-affected zones (HAZ) and a weaker joint. On the other hand, the rate at which welding is done is directly proportional to the amount of heat input; high speed reduces the duration of heat uptake, decreasing heat input, and, accordingly, resulting in a failure to attain full fusion or strong bonding [26].

In addition to these basic relationships, a correlation between the welding current and the welding speed has significant effects on the microstructural properties in the area of the weld. Overheating due to a strong current and low speed may cause grains to grow rough and reduce mechanical strength [27]. Conversely, low penetration and deficiency of fusion due to a lack of sufficient heat input may occur, caused by less strong electric current or high speed, which eventually leads to low tensile strength. Contour plots (Figures 5b, 5c, 5d) show significant parameter coupling. A strong welding current and low welding speed increased heat input drastically, correlating with porosity, a larger FZ, and reduced mechanical performance. Higher wire feed speed mitigated burn-off tendencies at stronger I, stabilising arc length. A proper coordination of travel speed and deposition rate prevented underfill and avoided surface turbulence. Elliptical contours confirm nonlinear behaviour in accordance with the standard CCD patterns presented in [24].

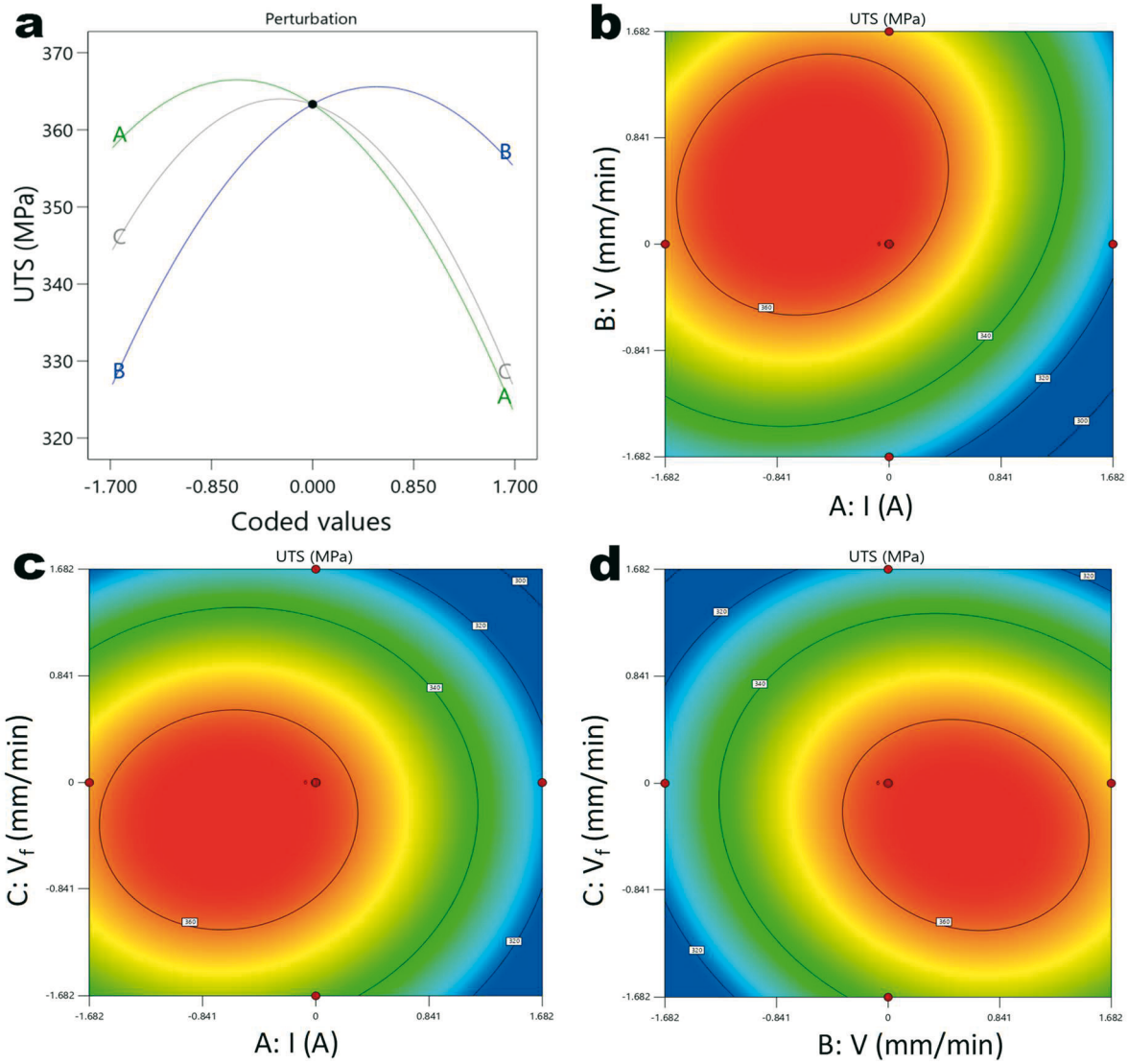

Fig. 5 Plots a) Perturbation b) AB interaction c) AC interaction d) BC interaction

The results demonstrate the importance of accurate optimisation in the welding process. The highly developed statistical and experimental design techniques, like the CCD, provide a powerful tool to determine the best set of process parameters [28]. The methods enable the maximum UTS to be achieved in the weld and a significant reduction in defects at the same time. The perturbation and contour studies provide useful information on the effects of individual parameters and their interaction, which provides a basis for decision-making to achieve improved weld quality and benefits of higher fatigue and to satisfy the mechanical performance goals of a particular project. Heat input is found to be a key aspect of strength loss during welding; an added amount of heat in the form of high heat input produces greater depths of softening and restricts the amount of strengthening components and precipitate particles in the weld area. High heat input will enhance the rate of growth in the HAZ, which will, in turn, cause significant yield strength and tensile strength to be lost in the welded joint. These observations confirm the need to carefully regulate and sustain the heat input to maintain the desirable mechanical properties of the weld [29].

3.5 Optimised welding process parameter

Once the parameter values were coded, the optimum coded parameter value optimisation was carried out, and the optimum coded parameter values were, in turn, converted back to actual values to be used in practice. Table 6 gives a complete comparison between the predicted

parameters as attained after the optimisation process and the experimentally determined parameters in validation trials. The optimisation characterised tensile strength as the response variable and presented a maximisation problem, which aimed at obtaining the highest possible UTS in the specified welding setup. The results of the experimental validation of the optimised parameters showed good agreement with the predicted results. Validation was done at I = 180 A, V = 120 mm/min, and V_f = 500 mm/min, giving UTS = 366 MPa, which is close to the model prediction of UTS = 371 MPa. The obtained results, which are shown in Table 6, support the capability of the model to represent the thermal-mechanical dynamics that governs the CMT welding of AA7075. The agreement between the experimental and the predicted UTS values ensures the accuracy and reliability of the RSM-based optimisation process. Consequently, the results support the quality control of the welding parameters to attain good mechanical properties. The correlation between data in experiments and the RSM-based prediction justifies the effectiveness of the empirical model used to account for the complex welding process. Furthermore, the findings provide way to the high tensile strength and offer a good understanding of the complex relations between the welding conditions and mechanical characteristics.

Table 6 Optimised welding process parameters

Parameters	Units	Experimental	Predicted
I	Amps	180	174
V	mm/min	120	127
V_f	mm/min	1500	1503
	UTS (MPa)	366	371

3.6 Microstructural analysis

As observed, the microphotographs of the microstructure showed a small extent of porosity in the fusion zone (FZ). This observation is similar to those of Elrefaey [30], who found few minor pores present in the FZ of CMT-welded joints produced under similar welding conditions; in Elrefaey's study, surface cleaning before welding was done using acetone. On the other hand, Ipekoğlu's study [31] revealed that there is relative porosity formation in the FZ, but in that study, only mechanical cleaning with a metal brush was done. Therefore, the increased porosity in the FZ is likely due to inadequate cleaning methods used before welding, which failed to completely remove the oxide layer and other contaminants. Additionally, the higher cooling rates after welding in Ipekoğlu's study may have contributed to the extensive pore formation.

SEM analysis provided detailed insights into the metallurgical changes caused by CMT. The microstructure of BM in Figure 6a shows fine equiaxed grains produced through rolling, with homogeneously distributed $MgZn_2$ precipitates responsible for high strength in the T6 condition [32,33]. The latter is mostly attributable to the effectiveness of their contribution to restricting the motion of dislocations and to contributing effectively to precipitation hardening, which is the strengthening process. In addition, the micrograph reveals the occurrence of distinct intermetallic particles present in the distribution in an inhomogeneous pattern; the intermetallic particles are found to be iron- and silicon-enriched. Following the research findings documented in earlier publications [32–34], the mentioned particles have specifically been termed phases of Al_7Cu_2Fe, $Al_{12}Fe_3Si$, and Mg_2Si. Although these intermetallic compounds do contribute to enhancing the general strength of the alloy, it should be noted that their existence in the boundary locations of the grains can become a potential stress concentrator. In that case, if the material is exposed to mechanical loading, cracking may be initiated.

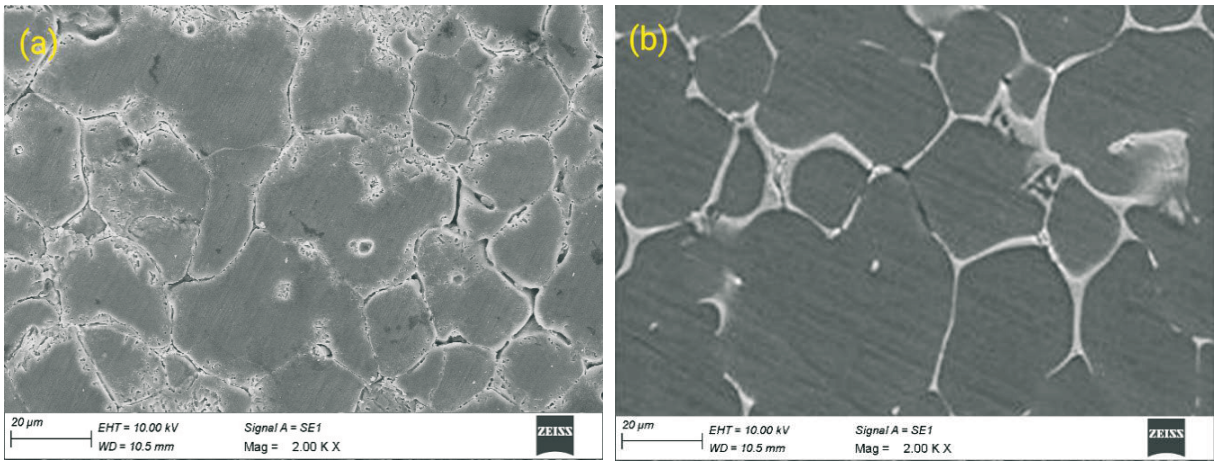

Fig. 6 SEM microstructures of a) Base metal AA7075 b) Fusion zone of specimen16

In CMT welding, the localised heat input causes the microstructure to change drastically. The fusion zone (Figure 6b) exhibited dendritic solidification morphology, complete dissolution of $MgZn_2$ precipitates, solute segregation to inter-dendritic regions, and coarsened secondary phases at grain boundaries. This change in morphology is a direct result of full melting and re-solidification under thermal gradients. The high peak temperatures in the FZ are above the solvus temperature of $MgZn_2$, causing dissolution of these strengthening precipitates. Since no post-weld ageing process was used, the lack of re-precipitation results in a softened microstructure with decreased strength and hardness. Rapid cooling inherent in CMT prevented extensive grain growth compared to conventional MIG, which is in accordance with prior CMT studies on Al–Mg–Zn alloys [35]. The grain size analysis of ASTM E112 revealed progressive coarsening from BM to HAZ to FZ. Segregation of zinc and magnesium during solidification contributed to reduced strengthening, which is consistent with the element-loss studies [36,37]. Besides the aforementioned, the low heat input, along with the controlled droplet transfer that is intrinsic in the CMT process, allows for a type of directional solidification. This specific phenomenon is of enormous importance since it efficiently reduces the percentages of porosity and the hazards involved in hot cracking during the welding process. Nonetheless, it is worth noting that the redistribution and segregation of the alloying elements, such as Zn, Mg, and Cu, during the solidification process open up a possibility of causing the unintended formation of secondary eutectic phases. Such phases have a tendency to form along the inter-dendritic regions. The formation of eutectic phases may s adversely affect the mechanical performance of the resultant weld joint.

3.7 Hardness survey

The microhardness distribution along different weld zones, shown in Fig. 7, was measured using the Vickers microhardness tester. In Figure 7, the red line (Exp. No 16) represents the specimen that had the highest tensile strength value, and the blue line (Exp. No 6) represents the specimen that had the lowest tensile strength value.

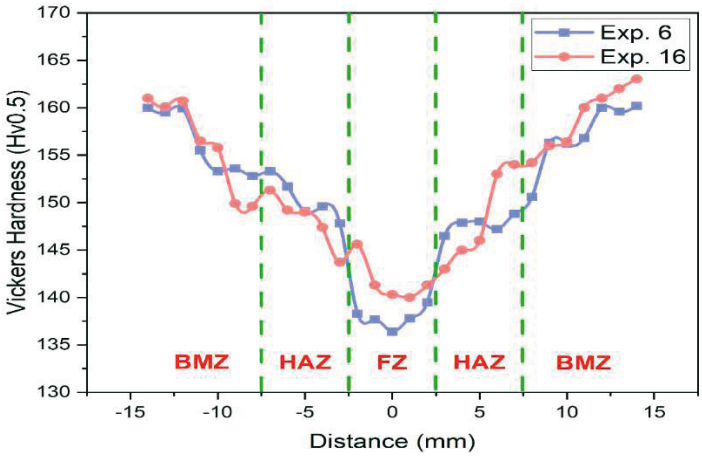

Fig. 7 Hardness distribution

The hardness profile exhibited the expected gradient for 7xxx aluminium welds; BMZ: 164–171 HV0.5 (retained T6 precipitation hardening); HAZ: 147–55 HV0.5 (partial dissolution and over-ageing of precipitates); and FZ: 140–145 HV0.5 (solute loss, precipitate dissolution, and dendritic morphology). The observed trends agree with the hardness behaviour reported for the CMT-welded AA5083 and AA6061 in [35] and TIG/GTAW-welded AA7075 in [36]. In the FZ, the elements are a mixture of the filler metal and dilution from the BM. The amount of strengthening elements, zinc and magnesium, decreases significantly in the FZ, as these elements tend to evaporate during the welding process [36-38]. The chemical composition of the FZ, in atomic percent, was found to be 1.83 Mg, 2.07 Zn, 0.28 Cu, and 95.82 Al. After the melting and solidification process, the alloy forms a supersaturated solution, with only a few particles precipitating from this solid solution. The softening in FZ is attributed to the dissolution of dizinc magnesium ($MgZn_2$) and magnesium silicide (Mg_2Si) strengthening phases, evaporation of zinc and magnesium during welding [37], solid-solution supersaturation without ageing, coarser grain morphology, and inter-dendritic segregation. Additionally, the grain size in the FZ increases, compared to BM, following solidification. Therefore, the reduced microhardness in the FZ is attributed to the smaller amount of alloying elements, the absence of sufficient precipitates, and grain coarsening. The moderate width of the HAZ and refined morphology in the FZ confirm the advantages of the CMT process relative to conventional fusion welding techniques regarding the heat input.

As shown in Fig. 7, the hardness profile will be progressive, as predicted (i.e., weld metal (WM), heat-affected zone (HAZ)). The similar pattern was recorded by Kang et al. [37]. Such a hardness gradient is mostly because it results from the welding process, bringing about microstructural changes. Specifically, the fine precipitates in the HAZ greatly contribute to hardness, and even though they are somewhat dissolved when welding is done, the fine precipitates are effective in increasing the local hardness. The greatest challenge is to retain the characteristic properties of the base metal's original T6 temper. The T6 temper refers to the solution heat treatment and subsequent artificial ageing, which yields a fine, homogeneous spread of strengthening $MgZn_2$ precipitates throughout the alpha matrix. This microstructure enables the BM to have high hardness and mechanical strength, but it makes little difference at distances that are not usually in the proximity to the thermal effects of welding. The effect of the observed hardness gradient is the thermal and metallurgical transformation across the weldment [38]. The strengthening precipitates dissolve, and coarser grains grow during welding in the FZ because of higher welding temperatures [39]. On the other hand, the longer the distance to the fusion line, the smaller the thermal gradient, which allows partial reprecipitation of dizinc magnesium ($MgZn_2$) in the HAZ. It is the reprecipitation in association with solid-solution effects that remains and has contributed to the slow restoration of hardness in these areas.

4. Conclusions

In this study, a critical examination of the cold metal transfer (CMT) welding parameters and their effect on the mechanical performance and microstructure of AA7075 alloy joints was carried out. The welding current (I), welding speed (V), and wire feed speed (V_f) were optimised using response surface methodology (RSM) and central composite design (CCD), and their impacts were discussed critically. Based on the extended investigation, the following conclusions have been drawn:

- The CMT welding process, a process with greatly reduced heat input, was effectively tested on AA7075. It produced welds of refined microarchitecture with narrower softening regions than those produced by conventional fusion welding. The initial experiments and tests confirmed that there were critical parameter limits that were needed to prevent porosity, the absence of fusion, and the burning of filler.
- As RSM showed, the welding current (I) had the highest impact on ultimate tensile strength (UTS), followed in descending order by the welding speed (V) and the wire feed speed (V_f). There was a strong nonlinear interaction, particularly between I and V as well as between I and V_f, which necessitated balancing heat input and the deposition rate to produce high-quality welds.
- The created empirical model displayed a high level of predictive power with a high level of statistical significance ($p < 0.0001$), high R^2 convergence, and a low level of lack of fit. Experimental confirmation of this model at I = 180 A, V = 120 mm/min, and V_f = 1500 mm/min gave a measured UTS of 366 MPa and compared well with a predicted model UTS of 371 MPa.
- Microstructural analysis showed that there were wide-ranging metallurgical changes in the fusion zone (FZ) in the form of dissolution of $MgZn_2$ precipitates, dendritic solidification, inter-dendritic segregation of Zn and Mg, and moderate grain coarsening. The high cooling rate of CMT restricted excessive growth of the grain, which gave rise to a finer structure compared to the ordinary GMAW/MIG.
- The profile of hardness throughout the weldment showed the desired gradient, with the lowest one observed in the FZ (140-145 HV0.5), moderate in the HAZ (147-155 HV0.5), and the highest in the base metal (164-171 HV0.5). These values are closely associated with the dissolution of precipitate, over-ageing at the location of HAZ, and with the effect of solute evaporation in the fusion zone.
- In general, the findings indicate that CMT is one of the most suitable welding methods for AA7075. If the process parameters are optimised, CMT-welded joints have better mechanical performance, better-controlled microstructure and heat input levels, and more homogeneous performance. The results form a parameter window that has proved to be efficient in obtaining high-strength, defect-minimised welds in high-strength aluminium alloys.

REFERENCES

[1] Kang, M, Kim, C, "A Review of Joining Processes for High Strength 7xxx Series Aluminum Alloys," Journal of Welding and Joining, vol. 35, (2017), pp. 79-88. https://doi.org/10.5781/JWJ.2017.35.6.12

[2] Fouad, Ramy A, Mohamed IA Habba, Yousef GY Elshaghoul, Mohamed M. El-Sayed Seleman, Khalid M. Hafez, F. S. Hamid, Waheed S. Barakat. "The influence of various welding wires on microstructure and mechanical characteristics of AA7075 Al-alloy welded by TIG process," Journal of Scientific Reports. vol. 14, (2024), pp.19023. https://doi.org/10.1038/s41598-024-69227-4

[3] Pickin, C. G,Ken Young, "Evaluation of cold metal transfer (CMT) process for welding aluminium alloy," Journal of Science and Technology of Welding and Joining, vol. 11, (2006), pp. 583-585. https://doi.org/10.1179/174329306X120886

[4] Indra Jeet Singh, Qasim Murtaza, Paras kumar, "A comprehensive review on effect of cold metal transfer welding parameters on dissimilar and similar metal welding," Journal of Engineering Research, (2023). https://doi.org/10.1016/j.jer.2023.12.009

[5] Singh, I.J., Murtaza, Q., Kumar, P, "Effect of CMT Welding Process Parameters on the Microstructural and Mechanical Properties of Dissimilar Aluminum Alloys of AA8011 and AA6061," Transactions of the Indian Institute of Metals, vol. 78, (2025). https://doi.org/10.1007/s12666-024-03471-0

[6] Zhao., Yili, Furong Chen, Silong Cao, Chao Chen, Ruijun Xie, "Effect of CMT welding heat input on microstructure and properties of 2A14 aluminum alloy joint," Journal of Metals, vol. 12, (2022), pp. 2100. https://doi.org/10.3390/met12122100

[7] Kumar., Sanjay, Pravin K. Singh, and Shashi B. Prasad D Patel, "Optimization of welding parameters of GTAW using response surface methodology," Journal of Scientific Bulletin Series-D, vol. 79, (2017), pp.119-132.

[8] Ravichandran., Manickam, Mokkaiya Thirunavukkarasu, Shanmugam Sathish, and Veeramani Anandakrishnan,"Optimization of welding parameters to attain maximum strength in friction stir welded AA7075 joints," Journal of Materials Testing, vol. 58, (2022), pp. 206-210. https://doi.org/10.3139/120.110838

[9] Kosturek., Robert, Janusz Torzewski, Marcin Wachowski, Lucjan Śnieżek, "Effect of welding parameters on mechanical properties and microstructure of friction stir welded AA7075-T651 aluminum alloy butt joints," Journal of Materials, vol. 15, (2022), pp.5950. https://doi.org/10.3390/ma15175950

[10] Balakrishnan., M, C. Leitão, E. Arruti, E. Aldanondo, D. M. Rodrigues, "Influence of pin imperfections on the tensile and fatigue behaviour of AA 7075-T6 friction stir lap welds," The International Journal of Advanced Manufacturing Technology, vol. 97, (2018), pp. 3129-3139. https://doi.org/10.1007/s00170-018-2172-x

[11] Wang Kekuan, Liu Jian, Duan Ruibin, Cui Wanting, Niu Huli, Li Liangyu, Yue Jianfeng, "Current waveform effects on AC-CMT arc welding of 7075 Al alloy with addition of ER7075 wire," Welding in the World, (2024), pp. 1-21. https://doi.org/10.1007/s40194-024-01894-3

[12] Omiyale, Babatunde Olamide, Ikeoluwa Ireoluwa Ogedengbe, Temitope Olumide Olugbade, Akeem Abiodun Rasheed, Akinola Ogbeyemi, Peter Kayode Farayibi. "Cold metal transfer WAAM of aluminum alloys: influence of processing parameters", The International Journal of Advanced Manufacturing Technology, vol. 136 (2025), pp. 1967-1987. https://doi.org/10.1007/s00170-024-14989-4

[13] CMT - The coldwelding process for premium quality. (2024). fronius.com. https://www.fronius.com/en-us/usa/welding-technology/world-of-welding/fronius-welding-processes/cmt-alt.

[14] Sasi Lakshmikhanth. R, Lakshminarayanan. A.K, "On the mechanical, microstructural, and corrosion properties of pulsed gas tungsten arc and friction stir welded RZ5 rare earth grade magnesium alloy", Materials Research Express, vol. 9, (2022), 126507. https://doi.org/10.1088/2053-1591/aca6c7

[15] Sasi Lakshmikhanth R, Subbaiah. K, "Mechanical Properties and Microstructural Characterization of Dissimilar Friction Stir Welded AA5083 and AA6061 Aluminium Alloys", Mechanika, vol. 26(6), (2020), pp. 545-552. https://doi.org/10.5755/j01.mech.26.6.25255

[16] Ramarajan. A, K. Jayakumar, "Influence of pulsed TIG welding process parameters on the mechanical characteristics of AA5083 with AA6082 weldments", Materials Research Express, vol. 10, (2023), 026504. https://doi.org/10.1088/2053-1591/acb682

[17] Wu, S. C., Xiao Yu, R. Z. Zuo, W. H. Zhang, H. L. Xie, J. Z. Jiang, "Porosity, element loss, and strength model on softening behavior of hybrid laser arc welded Al-Zn-Mg-Cu alloy with synchrotron radiation analysis," Welding Journal, vol. 3, (2013), pp. 64-71.

[18] SivashanmugamM, K. A. Kumar, R. Kajabanthanavas, M. A. E. Ahaned, "Effect of process parameters on tensile strength in gas metal arc welding joints AA7075-T6 aluminium alloy by using regression and response surface model," International Journal of Research in Engineering and Technology, vol. 3, (2014), pp. 162-166. https://doi.org/10.15623/ijret.2014.0302029

[19] Sunny., Kora T., Nanda Naik Korra, M. Vasudevan, B. Arivazhagan, "Parameter optimization and experimental validation of A-TIG welding of super austenitic stainless steel AISI 904L using response surface methodology," Proceedings of the Institution of Mechanical Engineers, Part E, Journal of Process Mechanical Engineering, vol. 236, (2022), pp.2608-2617. https://doi.org/10.1177/09544089221095671

[20] Bae., Jin-Hee, Yeong-Do Park, Mokyoung Lee, "Optimization of welding parameters for resistance spot welding of AA3003 to galvanized DP780 steel using response surface methodology," International Journal of Automotive Technology, vol. 22, (2021), pp. 585-593. https://doi.org/10.1007/s12239-021-0055-x

[21] Desh Raj, Ranganath M. Singari, M. Vipin, "Study and analyses of arc length correction and mechanical properties on weld bead geometry for AA6061T6 by CMT process", Materials Today: Proceedings, 2022, vol. 56(6), pp 3475-3483. https://doi.org/10.1016/j.matpr.2021.11.122

[22] Rajesh Kannan, A., Siva Shanmugam, N., Naveenkumar, S, "Effect of Arc Length Correction on Weld Bead Geometry and Mechanical Properties of AISI 316L Weldments by Cold Metal Transfer (CMT) Process", Materials Today: Proceedings, 2019, Vol. 18(7), pp. 3916-3921. https://doi.org/10.1016/j.matpr.2019.07.331

[23] Rajeev, G. P., Kamaraj, M., & Bakshi, S. R. (2019). "Effect of correction parameters on deposition characteristics in cold metal transfer welding," Materials and Manufacturing Processes, 34(11), pp. 1205-1216. https://doi.org/10.1080/10426914.2019.1628260

[24] Thilagham., Kancheepuram Thirumal, Lekshmy Premachandran Ladha, Anand Prakash Tiwary, Munde Kashinath Haribhau, Darade Pradipkumar Dudhajirao, Shailseh Ranjan Kumar, "Developing a mathematical model for predicting ultimate tensile strength to identify optimal machining parameters" International Journal of Electrical and Computer Engineering, vol. 14, (2024), pp. 7116-7125. https://doi.org/10.11591/ijece.v14i6.pp7116-7125

[25] Prashantha, S., B. R. Omkaresh, "Influence of Welding Parameters on Weld Timings, Temperature Variation and Mechanical Strength of Friction Stir Welded AA6061 and AA6082 Alloy," Journal of Mines, Metals and Fuels, (2024), pp. 347-355. https://doi.org/10.18311/jmmf/2024/44426

[26] Abima,. Cynthia S., Stephen A. Akinlabi, Nkosinathi Madushele, Esther T. Akinlabi, "Process Parameters Optimization for GMA Welding of AISI 1008 Steel Joints for Optimal Tensile Strength," Journal of Composite and Advanced Materials/Revue des Composites et des MatériauxAvancés, vol. 31, (2021), pp. 349-354. https://doi.org/10.18280/rcma.310606

[27] Subramanian., Raja, Balaji Natarajan, Balasubramanian Kaliyaperumal,Rajendran Chinnasamy, "Effect of MIG welding process parameters on microstructure and tensile behavior of hastelloy C276 using response surface methodology," Materials Research Express, vol. 6, (2019), pp. 066540. https://doi.org/10.1088/2053-1591/ab093a

[28] Masuyama., Fujimitsu, Tomiko Yamaguchi, "New ferritic steel beyond Grade 92 and its creep degradation assessment by hardness method for Grade 91," In Pressure Technology, American Society of Mechanical Engineers, vol. 40740, (2014), pp. 54-61. https://doi.org/10.1115/ETAM2014-1007

[29] Zhu., Xiaohu, Rui Wang, Lin Wang, Mengmeng Liu, Songmo Li, "Effect of Rotational Shear and Heat Input on the Microstructure and Mechanical Properties of Large-Diameter 6061 Aluminium Alloy Additive Friction Stir Deposition," Journal of Crystals, vol. 14, (2024), pp. 581. https://doi.org/10.3390/cryst14070581

[30] Elrefaey. A, "Effectiveness of cold metal transfer process for welding 7075 aluminium alloys," Journal of Science and Technology of Welding and Joining, vol. 20, (2015), pp.280-285. https://doi.org/10.1179/1362171815Y.0000000017

[31] İpekoğlu., Güven, Gürel Çam, "Formation of weld defects in cold metal transfer arc welded 7075-T6 plates and its effect on joint performance," In IOP Conference Series, Materials Science and Engineering, vol. 629, (2019), pp. 012007. https://doi.org/10.1088/1757-899X/629/1/012007

[32] İpekoğlu., Güven, B. Gören Kıral, Seçil Erim, and Gürel Çam, "Investigation of the effect of temper condition on friction stir weldability of AA7075 Al-alloy plates," Materials and Technology, vol. 46, (2012), pp.627-632.

[33] İpekoğlu., Güven, Seçil Erim, and Gürel Çam, "Effects of temper condition and post weld heat treatment on the microstructure and mechanical properties of friction stir butt-welded AA7075 Al alloy plates," The International Journal of Advanced Manufacturing Technology, vol. 70, (2014), pp. 201-213. https://doi.org/10.1007/s00170-013-5255-8

[34] İpekoğlu., Güven, Gürel Çam, "Formation of weld defects in cold metal transfer arc welded 7075-T6 plates and its effect on joint performance," In IOP Conference Series, Journal of Materials Science and Engineering, IOP Publishing, vol. 629, (2019), pp. 012007. https://doi.org/10.1088/1757-899X/629/1/012007

[35] Gungor, Beytullah, Erdinc Kaluc, Emel Taban, S. I. K. Aydin, "Mechanical and microstructural properties of robotic Cold Metal Transfer (CMT) welded 5083-H111 and 6082-T651 aluminum alloys," Journal of Materials & Design, vol. 54, (2014), pp. 207-211. https://doi.org/10.1016/j.matdes.2013.08.018

[36] Sivashanmugam., M, T. Kumar, M. Sathishkumar, "Investigation of microstructure and mechanical properties of GTAW and GMAW joints on AA7075 aluminum alloy," In Frontiers in Automobile and Mechanical Engineering, IEEE, (2010), pp. 241-246. https://doi.org/10.1109/FAME.2010.5714843

[37] Kang, Y, Seo, K, Lee, J.-H, Oh, C.-Y, Lee, S.G, "Effect of Post-Weld Heat Treatment Temperature on the Mechanical Properties and Microstructure of Weld Heat-Affected Zone of 2.25 Cr-1Mo Steel," Journal of Welding and Joining, vol. 41, (2023), pp. 175-180. https://doi.org/10.5781/JWJ.2023.41.3.5

[38] Yoo, Seonghoon., Yoona Lee, Myeonghawn Choi, Hyunbin Nam, Sangyong Nam,Namhyun Kang, "Enhancing Microstructural and Mechanical Properties of Ferrous Medium-Entropy Alloy through Cu Addition and Post-Weld Heat Treatment in Gas Tungsten Arc Welding," Journals of Materials, vol. 17, (2023), pp.181. https://doi.org/10.3390/ma17010181

[39] Rifat Bin Zakir, Demario Broderick, Heshmat Aglan, "Microstructural Origin of Hardness in Thermite Welded Rails," Microscopy and Microanalysis, vol. 29, (2023), pp. 204-206. https://doi.org/10.1093/micmic/ozad067.090

Submitted: 23.6.2025

Accepted: 15.01.2026

R. Venkatesh
Research Scholar, Department of Mechanical Engineering,
Sri Sivasubramaniya Nadar College of Engineering, Chennai-603110 and
Assistant Professor, Department of Mechanical Engineering, DMI College of Engineering, Chennai-600124, India

Dr. K. Jayakumar*
Associate Professor, Department of Mechanical Engineering,
Sri Sivasubramaniya Nadar College of Engineering, Chennai-603110, India

*Corresponding author:
kjayakumar@ssn.edu.in